The Digital Elliptic Filter—A Compact Sharp-Cutoff Design for Wide Bandstop or Bandpass Requirements

M. C. HORTON, MEMBER, IEEE, AND R. J. WENZEL, MEMBER, IEEE

Abstract—**Detailed design procedures are presented for a practical elliptic-function filter form capable of achieving high selectivity in a very compact configuration. This filter form, called the digital elliptic because of its digital construction and elliptic function response, can provide either bandpass or bandstop characteristics. Examples are given to illustrate typical design procedures for both bandpass and bandstop applications. Experimental results are presented for an octave bandstop design.**

Introduction

RECENTLY, the application of modern network techniques to distributed lines [1]–[5] has permitted the exact design of microwave TEM filters by using methods employed in the exact synthesis of lumped element filters. The relationship between a lumped element prototype filter and its distributed element counterpart is accomplished by employing Richards' [6] tangent transformation (1). Using this transform, a shorted quarter-wavelength stub is represented as an inductor L and an open stub is represented as a capacitor C. The "unit element," a quarter-wavelength of line, can also be represented and used in the theory but it has no lumped element counterpart.

Several previous papers have covered in detail the design of distributed filters having equal-ripple response, or maximally flat response, in the passband only [1]–[5]. Such lumped element filter prototypes are usually referred to as Chebyshev or Butterworth, respectively. A lumped element prototype which has sharper cutoff characteristics for a given number of sections is the well-known Cauer parameter or elliptic-function filter which exhibits equal-ripple response in both passband and stopband. Tables of element values are available for the simple design of such lumped element filters. This paper presents a simple exact design procedure for the construction of an elliptic-function distributed-line filter using the available tables. The procedure is a specific application of the general theory presented in a previous paper [7]. Because of the finger-like appearance of the structure, the new filter has been termed the digital elliptic. For wide bandwidth designs (greater than 30 percent), either distributed bandpass or bandstop, the digital elliptic filter is an extremely compact microwave structure for attaining sharp cutoff characteristics.

Manuscript received September 6, 1966; revised December 22, 1966. This work was supported by the U. S. Army Electronics Laboratory, Fort Monmouth, N. J., under Contract DA 28-043 AMC-01869(E).

The authors are with The Bendix Corporation, Research Laboratories Division, Southfield, Mich.

The remainder of this paper presents the simple design procedure used in converting from the lumped element low-pass (or high-pass) prototype to the distributed element bandstop (or bandpass) realization, and gives example designs for both bandstop and bandpass filters. Test results are presented for an experimental model of an octave bandstop design. The paper concludes with a summary of the practical advantages and limitations of the digital elliptic filter.

Design Procedure

The low-pass and high-pass lumped element prototypes of an elliptic-function filter are shown in Fig. 1(a) and (b), respectively. Parallel resonant tank circuits in the series branches create transmission zeros, or attenuation peaks, in the stopband of each prototype at finite frequencies as shown in the response characteristics. The approximation problem for filters of this type which give equal-ripple response in both passband and stopband has been solved and the synthesis of appropriate element values may be found in published tables [8]–[11]. Also presented in these tables are the finite frequencies of zero transmission and the ratio of cutoff frequencies between regions of high and low transmission.

Conversion from the lumped element frequency variable Ω to the distributed element frequency variable $\omega=2\pi f$ is accomplished through Richards' transformation,

$$\Omega = \tan\frac{\pi\omega}{2\omega_0} = \tan\frac{\pi f}{2f_0} \tag{1}$$

where $\omega_0=2\pi f_0$ is the frequency for which all distributed TEM lines are one quarter-wave in length. This transformation involves only a ratio of distributed frequencies, i.e., $\omega/\omega_0=f/f_0$. Since most desired response characteristics are specified in terms of f rather than ω, the subsequent design of digital elliptic filters, including characteristics and equations, will be given in terms of f. The entire positive frequency range in Ω is mapped by the transformation into the positive range in f from zero to f_0. Because of the repetitive nature of the tangent function, the response characteristic then repeats on an interval of $2f_0$ producing response "windows" as shown in Fig. 2(a) and (b).

Physically, the conversion using (1) implies that each inductor in the prototype be replaced by a shorted quarter-

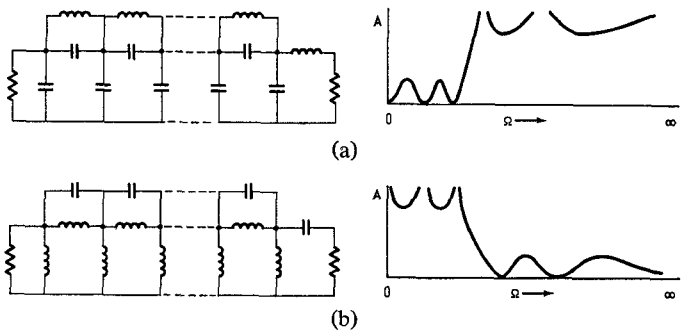

Fig. 1. Elliptic function prototype filter networks and attenuation characteristics: (a) prototype low-pass, and (b) prototype high-pass.

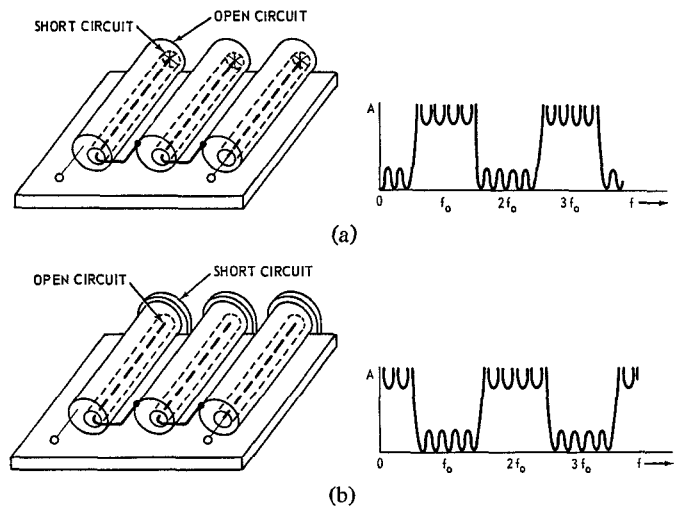

Fig. 2. Digital elliptic microwave filter configurations and responses for (a) distributed bandstop designs, and (b) distributed bandpass designs.

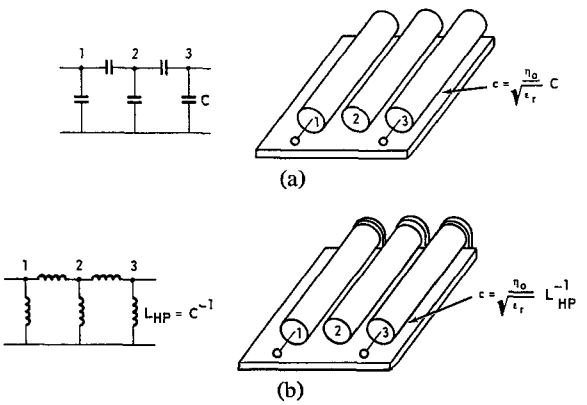

Fig. 3. Parallel conductor distributed representations of transformed lumped element prototype networks: (a) capacitive, and (b) inductive.

wave stub of normalized characteristic impedance given by the inductive prototype value, and that each capacitor be replaced by an open quarter-wave stub of normalized characteristic admittance given by the capacitive prototype value. Concentrating first on the low-pass prototype of Fig. 1(a), it has been pointed out [12]–[14] that the capacitive portion of this network is the lumped element representation of a parallel array of quarter-wavelength conductors above a ground plane, one conductor representing each ungrounded node in the prototype, as shown for a three-node network in Fig. 3(a). Further, all lumped element capacitance values, e.g., C in Fig. 3(a), are proportional to the respective "static capacitance" values c of the distributed line[1] such that $c=(\eta/\sqrt{\epsilon_r})C$, where $\eta=376.7/Z_0$ for a filter terminated in Z_0 ohms and ϵ_r is the relative dielectric constant of the medium. Again, glancing at Fig. 1(a), the inductances bridging each node and in series with the output port can be represented in the distributed parallel line system of Fig. 3(a) by incorporating shorted coaxial stubs within each line and attaching each stub center conductor to the next adjacent parallel line, as shown in the digital elliptic bandstop configuration of Fig. 2(a). The repetitious response of this filter with frequency f is the same as the prototype network response mapped by (1).

In similar manner, the inductive portion of the high-pass prototype network of Fig. 1(b) is represented in distributed form by a parallel array of conductors shorted at the far end as in Fig. 3(b). All distributed "static capacitance" values c are now related to the respective prototype inductance values L_{HP} by the proportional relation $c=(\eta/\sqrt{\epsilon_r})$ L_{HP}^{-1}. The bridging series capacitors are incorporated internally within the parallel conductors as open stubs. The resulting configuration and response of the digital elliptic bandpass filter is given in Fig. 2(b).

A. Prototype L-P (Microwave Bandstop)

The procedure for obtaining bandstop digital elliptic filter dimensions will be described briefly. Convenient charts [15]–[16] are used to design the prototype capacitive portion, i.e., the parallel conductor array. The bandwidth-normalized values of self and mutual "static capacitance" required for use with the referenced charts are obtained by multiplying the low-pass prototype capacitance values C by $(\eta/\sqrt{\epsilon_r})$, thus

$$c_{\text{chart}} = \frac{376.7}{Z_0\sqrt{\epsilon_r}} C. \tag{2}$$

The characteristic impedances of the shorted series stubs are given in terms of the low-pass prototype inductance values L by

$$\sqrt{\epsilon_r}\, Z_{\text{series stub}} = \sqrt{\epsilon_r}\, Z_0 L, \tag{3}$$

and physical dimensions can be obtained from nomographs [17].

[1] Note that c as defined here is dimensionless, and is actually the ratio of static capacitance between conductors per unit length to the dielectric constant of the medium (this ratio is independent of the dielectric medium and depends only on cross-sectional geometry) [13].

B. Prototype H-P (Microwave Bandpass)

The normalized self and mutual static capacitance values for the prototype inductive portion of the bandpass digital elliptic filter are obtained by dividing $\eta/\sqrt{\epsilon_r}$ by the high-pass prototype inductance values L_{HP} to give

$$c_{\text{chart}} = \frac{376.7}{Z_0\sqrt{\epsilon_r}} L_{HP}^{-1}, \tag{4}$$

and the characteristic impedances of the series open stubs are given in terms of the high-pass prototype capacitance values C_{HP} by

$$\sqrt{\epsilon_r}\, Z_{\text{series stub}} = \sqrt{\epsilon_r}\, Z_0 C_{HP}^{-1}. \tag{5}$$

All dimensions are obtained as in the *L-P* prototype by using the referenced charts and nomographs.

C. Bandwidth Scaling

The tables of prototype elliptic-function filter element values given in Saal and Ulbrich [8], and Saal [9] are normalized to a cutoff frequency of unity, $\Omega_c = 1$. Therefore, when a digital elliptic filter is constructed as described above, it will provide a stop or pass bandwidth of 100 percent (3 to 1) centered about the quarter-wave frequency f_0. Frequency scaling to other than 100 percent bandwidth can be achieved by dividing all prototype element values in (2)–(5) by a scaling constant Ω_c', which may be either greater or less than unity. This is equivalent to changing to a new bandwidth-scaled frequency variable Ω' given by

$$\Omega' = \Omega_c'\Omega = \tan\frac{\pi f'}{2f_0}. \tag{6}$$

Values of $\Omega_c' > 1$ give rise to a reduced bandwidth in the case of either a bandstop or bandpass filter, and $\Omega_c' < 1$ corresponds to increased bandwidth.[2] The scaling constant, from (1), is given by

$$\Omega_c' = \tan\frac{\pi f_{c1}'}{2f_0} = \tan\frac{\pi f_{c1}'}{f_{c1}' + f_{c2}'},$$

where f_{c1}' is the lower, and f_{c2}' is the higher desired bandedge cutoff frequency for either bandstop or bandpass digital elliptic filters. The resulting percentage bandwidth is given by [3]:

$$\%\text{BW} = 200\left(1 - \frac{2}{\pi}\tan^{-1}\Omega_c'\right).$$

The elliptic-function filter tables of Saal and Ulbrich [8] and Saal [9] list only low-pass prototype element values, C and L. The normalized-bandwidth high-pass prototype values, $L_{HP} = C^{-1}$ and $C_{HP} = L^{-1}$, are reciprocals of the low-pass prototype values. Thus the normalized-bandwidth high-pass prototype equations (4) and (5) become identical to those for the low-pass prototype equations (2) and (3). When bandwidth scaling is performed, the factor Ω_c' defined before, divides the low-pass prototype element values of (2) and (3) in a low-pass prototype design, and multiplies them in a high-pass prototype design.

The complete set of design equations for digital elliptic filters is given in Table I for handy reference. Equations are included for calculating bandwidth scaling factor Ω_c', and bandwidth-normalized prototype skirt selectivity factor Ω_s. The selectivity factor symbol (Ω_s), the low-pass capacitance and inductance symbols (C and L), and the maximum passband attenuation (A_D), and minimum stopband attenuation (A_s) symbols used in Table I are identical to those used in the tables of Saal and Ulbrich [8], and Saal [9].

Design Examples

A. Example I: Octave Bandstop Design

Assume that a bandstop filter is to be designed to meet the following specifications:

a) Passband cutoff frequencies of $f_{c1}' = 1.0$ GHz, $f_{c2}' = 2.0$ GHz.
b) Passband VSWR $\leq 1.6:1$.
c) Attenuation (A_s) to be ≥ 30 dB for 1.050 GHz $\leq f' \leq 1.950$ GHz; therefore $f_s' = 1.05$ GHz.

Referring to Table I, from (T-1),

$$\Omega_c' = \tan\frac{\pi f_{c1}'}{f_{c1}' + f_{c2}'} = \tan\frac{\pi}{3} = \sqrt{3}, \tag{7}$$

and from (T-3),

$$\Omega_s = \frac{\tan\dfrac{\pi f_s'}{f_{c1}' + f_{c2}'}}{\Omega_c'} = \frac{\tan 0.35\pi}{\sqrt{3}} = 1.13. \tag{8}$$

Note from specification c) and (8) that the tangent transformation increases the skirt selectivity factor of the distributed network relative to that of the lumped element prototype. A selectivity factor of 1.13 for the lumped element prototype corresponds to a selectivity factor of 1.05 for the distributed filter.

From the tables of Saal [9], a filter-type numbered *C-06-20c*, with modular angle $\theta = 66°$, provides the following characteristics which somewhat exceed the given specifications:

Maximum passband reflection coefficient $|\rho| = 0.20$ ($\text{VSWR}_{\max} = 1.5:1$).
Skirt selectivity factor $\Omega_s = 1.124$.
Minimum stopband attenuation $A_s = 31.5$ dB.
Frequencies of zero transmission $\Omega_4 = 1.143$; $\Omega_2 = 1.405$; $\Omega_\infty = \infty$.

The prototype circuit is shown in Fig. 4(a). From (6) normalized bandwidth-scaled real frequencies $(f'/f_0) = (2/\pi)$

[2] In all cases, percentage bandwidth (%BW) is bandwidth about f_0 and may be either a stopband or passband.

TABLE I

DESIGN EQUATIONS FOR DIGITAL ELLIPTIC FILTERS

	Prototype Low-Pass Microwave Bandstop	Prototype High-Pass Microwave Bandpass
	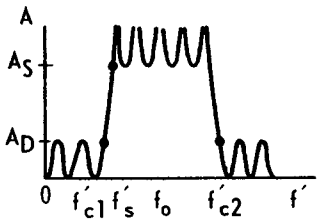	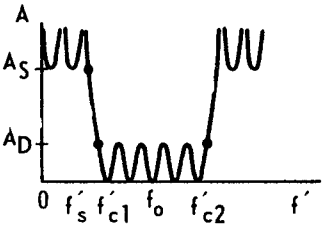
Bandwidth Scaling Factor, Ω_c'	$\Omega_c' = \tan\frac{\pi f_{c1}'}{2f_0} = \tan\frac{\pi f_{c1}'}{f_{c1}' + f_{c2}'}$ (T-1) $\%\ \text{BW} = 200\left(1 - \frac{2}{\pi}\tan^{-1}\Omega_c'\right)$ (T-2)	
Skirt Selectivity Factor, Ω_s	$\Omega_s = \frac{\Omega_s'}{\Omega_c'} = \frac{\tan\frac{\pi f_s'}{2f_0}}{\Omega_c'}$ (T-3)	$\Omega_s = \frac{\Omega_c'}{\Omega_s'} = \frac{\Omega_c'}{\tan\frac{\pi f_s'}{2f_0}}$ (T-4)
Parallel Conductor Array	$c_{\text{chart}} = \frac{376.7}{\sqrt{\epsilon_r}Z_0}\frac{C}{\Omega_c'}$ (T-5)	$c_{\text{chart}} = \frac{376.7}{\sqrt{\epsilon_r}Z_0}C\Omega_c'$ (T-6)
Internal Series Stubs	$\sqrt{\epsilon_r}Z_{\text{ser stub}} = \sqrt{\epsilon_r}Z_0\frac{L}{\Omega_c'}$ (T-7)	$\sqrt{\epsilon_r}Z_{\text{ser. stub}} = \sqrt{\epsilon_r}Z_0L\Omega_c'$ (T-8)

A_D = maximum passband attenuation level in dB.
A_S = Minimum stopband attenuation level in dB.
f_s' = Lower-edge frequency for which the attenuation is A_S.
f_{c1}' = Lower-edge passband cutoff frequency.
f_{c2}' = Higher-edge passband cutoff frequency.
$f_0 = (f_{c1}' + f_{c2}')/2$ = frequency for which the lines are quarter-wavelength.
Ω_s = Skirt selectivity parameter listed in Saal and Ulbrich [8] and Saal [9].
L, C = Low-pass prototype element values listed in Saal and Ulbrich [8] and Saal [9].
Z_0 = Characteristic terminating impedance (ohms).
ϵ_r = Relative dielectric constant of medium.
c_{chart} = "Static capacitance" to be found in charts [15], [16].
$\sqrt{\epsilon_r}Z_{\text{ser stub}}$ = Characteristic impedance to be found in chart [17].

$\tan^{-1}\Omega_c'\Omega$ corresponding to important response points are given by

$$\frac{f_{c1}'}{f_0} = \frac{2}{\pi}\tan^{-1}\sqrt{3}\,(1) = 0.667$$

$$\frac{f_s'}{f_0} = \frac{2}{\pi}\tan^{-1}\sqrt{3}\,(1.124) = 0.698$$

$$\frac{f_2'}{f_0} = \frac{2}{\pi}\tan^{-1}\sqrt{3}\,(1.143) = 0.703$$

$$\frac{f_4'}{f_0} = \frac{2}{\pi}\tan^{-1}\sqrt{3}\,(1.405) = 0.752$$

$$\frac{f_\infty'}{f_0} = \frac{2}{\pi}\tan^{-1}\infty = 1.000.$$

The octave bandwidth theoretical response characteristic is shown in Fig. 4(b). The actual distributed filter selectivity factor is

$$\frac{f_s'}{f_{c1}'} = \frac{0.698}{0.667} = 1.045. \tag{9}$$

For a 50-ohm realization, the self and mutual static capacitance values are obtained by direct substitution in (T-5) and the series stub impedance values likewise from (T-7). The appropriate static capacitance network is shown in Fig. 4(c), along with the stub impedance values. To enable the practical construction of the series stubs, a dielectric constant larger than that used for the coupled lines is desirable. With air-loaded coupled lines, Teflon ($\sqrt{\epsilon_r} = 1.44$) provides a convenient dielectric.

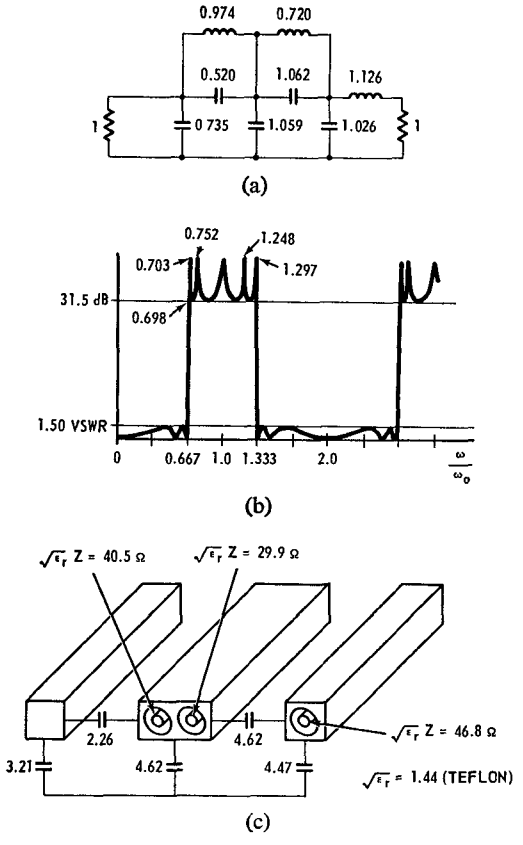

Fig. 4. Octave bandstop digital elliptic design. (a) Low-pass prototype element values. (b) Theoretical response characteristic. (c) Static capacitance values and series stub impedances.

Dimensions for the coupled-line portion of the filter are determined as for interdigital filters as described by Matthaei [18]. Thus, for a rectangular bar realization, $(s_{k,k+1})/b$ is determined directly from Fig. 3 of Getsinger [15] using $c_{m(k,k+1)}$, and

$$\frac{w_k}{b} = \frac{1}{2}\left(1 - \frac{t}{b}\right)\left[\frac{1}{2}c_{sk} - (c_{fe})_{k-1,k} - (c_{fe})_{k,k+1}\right] \quad (10)$$

is computed using the referenced charts. In the previous calculations

b = ground plane spacing,
t = line thickness,
$s_{k,k+1}$ = spacing between lines k and $k+1$,
w_k = width of the kth line,
c_{sk} = self capacitance of the kth line,
$c_{m(k,k+1)}$ = mutual capacitance between lines k and $k+1$,
$(c_{fe})_{k,k+1}$ = even-mode fringing capacitance between lines k and $k+1$ as determined from Fig. 3 of Getsinger [15].

Note that as $s/b \to \infty$, the corresponding $c_{fe} \to c_f$ where c_f is the fringing capacitance of an isolated line (Fig. 5 of Getsinger [15]). Thus for an N-line network

$$\frac{w_1}{b} = \frac{1}{2}\left(1 - \frac{t}{b}\right)\left[\frac{c_{s1}}{2} - c_f - (c_{fe})_{12}\right]$$

and

$$\frac{w_N}{b} = \frac{1}{2}\left(1 - \frac{t}{b}\right)\left[\frac{c_{sN}}{2} - (c_{fe})_{N-1,N} - c_f\right]. \quad (11)$$

Using the preceding equations, line dimensions for the bandstop filter of Fig. 4 were determined. The effect of the side walls was taken into account by using $c_{f0}(s_w/b)$ in place of c_f for the end lines as shown in Fig. 6 of Getsinger [15], where $s_w/2$ is the spacing between the end lines and the walls. A line drawing showing cross-sectional dimensions for $b = 0.500$ inch and $t = 0.200$ inch is given in Fig. 5(a). The diameter ratios for the series stubs were determined from the referenced nomograph [17]. Note that each w_k/b should satisfy the inequality

$$\frac{\frac{w_k}{b}}{1 - \frac{t}{b}} < 0.35 \quad (12)$$

as discussed by Getsinger [15]. If this is not satisfied (as was the case with the first line in the above example), the correction formula [15]

$$\frac{w_k'}{b} = \frac{0.07\left(1 - \frac{t}{b}\right) + \frac{w_k}{b}}{1.2} \quad (13)$$

can be used providing $0.1 < (w_k'/b)/[1-(t/b)] < 0.35$.

Using the cross-sectional dimensions of Fig. 5(a), an experimental model was constructed using quarter-wavelength lines at 1.5 GHz. Assembly sketches of the filter structure are shown in Fig. 5(b) and (c). Several junctions were mitered to reduce discontinuity effects. Line spacings were maintained by use of Teflon fiberglasss pacers as shown. Movable shorting slugs were provided to allow adjustment of the series stub lengths.

The measured response of the filter is shown in Fig. 6, and a photograph of the experimental model is shown in Fig. 7. The experimental results shown were obtained with no physical alterations other than adjustment of the series shorting slugs and matching of the connectors. The dielectric spacers provided a high degree of mechanical stability and did not appear to affect the electrical response. Junction effects and the nonzero width of the structure did not influence significantly the electrical performance.

B. Example II: Wide Bandpass Design (Pseudo High Pass)

Assume a wide bandpass filter is to be designed to satisfy the following specifications:

a) Passband cutoff frequencies $f_{c1}' = 1.0$ GHz, $f_{c2}' = 4.0$ GHz.
b) Passband VSWR less than 1.5:1.
c) Attenuation (A_s) to be ≥ 50 dB for $f' \leq 0.95$ GHz $(f_s' = 0.95$ GHz).

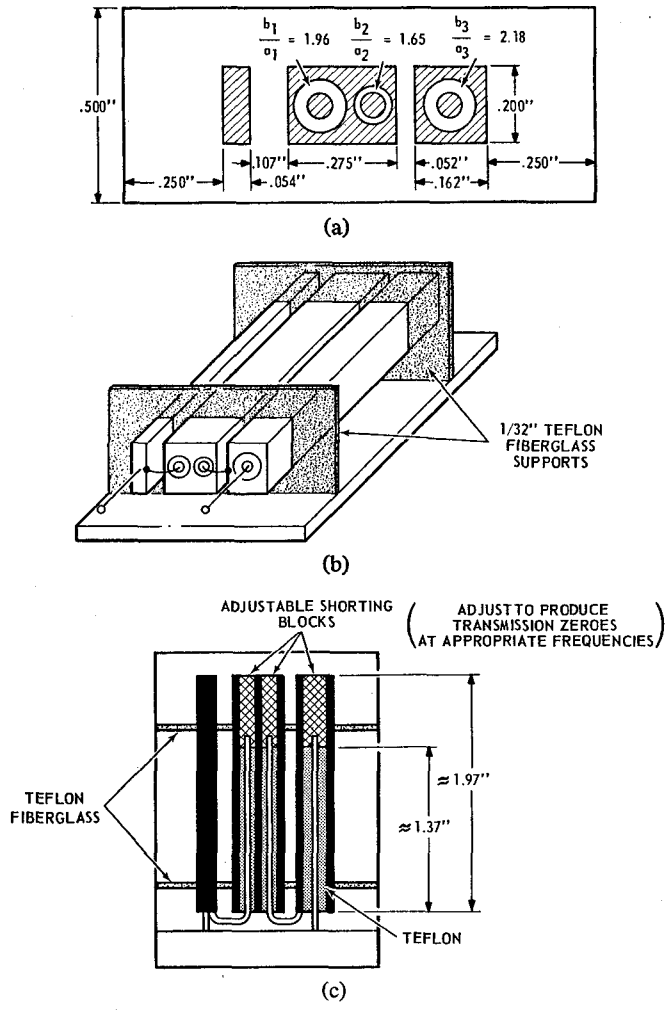

Fig. 5. Construction details of octave bandwidth digital elliptic filter. (a) Cross section. (b) Perspective view. (c) Plan view.

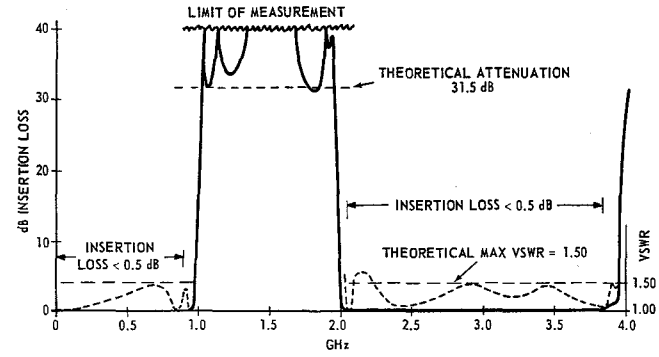

Fig. 6. Octave band digital elliptic measured response.

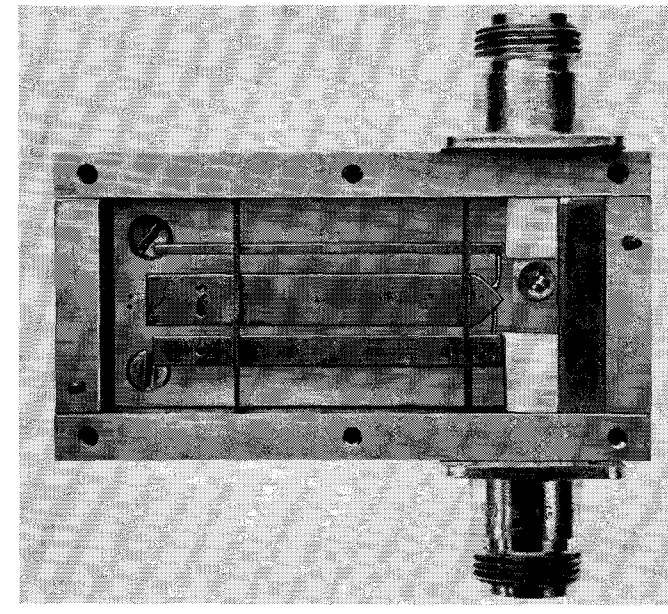

Fig. 7. Experimental octave bandstop digital elliptic filter.

From Table I, (T-1),

$$\Omega_c' = \tan\frac{\pi}{5} = 0.727 \tag{14}$$

and from (T-4),

$$\Omega_s = \frac{\Omega_c'}{\tan\dfrac{\pi(0.950)}{5}} = \frac{0.727}{0.680} = 1.07. \tag{15}$$

From Saal's tables [9] a filter-type numbered *C-09-15*, with modular angle $\theta = 70°$, provides the following satisfactory characteristics:

Maximum passband reflection coefficient $|\rho| = 0.15$ ($VSWR_{max} = 1.36:1$).
Skirt selectivity factor $\Omega_s = 1.064$.
Minimum stopband attenuation $A_s = 51.0$ dB.
Frequencies of zero transmission $\Omega_8 = 1.302$, $\Omega_6 = 1.069$, $\Omega_4 = 1.119$, $\Omega_2 = 2.094$, $\Omega_\infty = \infty$.

The low-pass prototype element values are shown in Fig. 8(a). The high-pass response characteristics are obtained by substituting $1/\bar{\Omega}$ for Ω as in the usual low-pass to high-pass transformation [19]. Therefore,

$$\bar{\Omega}_c = 1.0, \bar{\Omega}_s = 0.940, \bar{\Omega}_8 = 0.768, \bar{\Omega}_6 = 0.936,$$
$$\bar{\Omega}_4 = 0.895, \bar{\Omega}_2 = 0.478, \bar{\Omega}_\infty = 0.$$

Bandwidth-scaled distributed network frequencies, corresponding to important response points, are obtained by applying (6) and using the high-pass barred frequencies given by

$$\frac{\bar{f}'}{f_0} = \frac{2}{\pi}\tan^{-1}\Omega_c'\bar{\Omega}.$$

With $f_0 = 2.5$ GHz, the theoretical response characteristic is that shown in Fig. 8(b). The actual distributed filter selectivity factor is $\bar{f}_c/\bar{f}_s' = 1.047$. Note that in this example, because the tangent function is more nearly linear for small angles, the difference between the lumped element prototype selec-

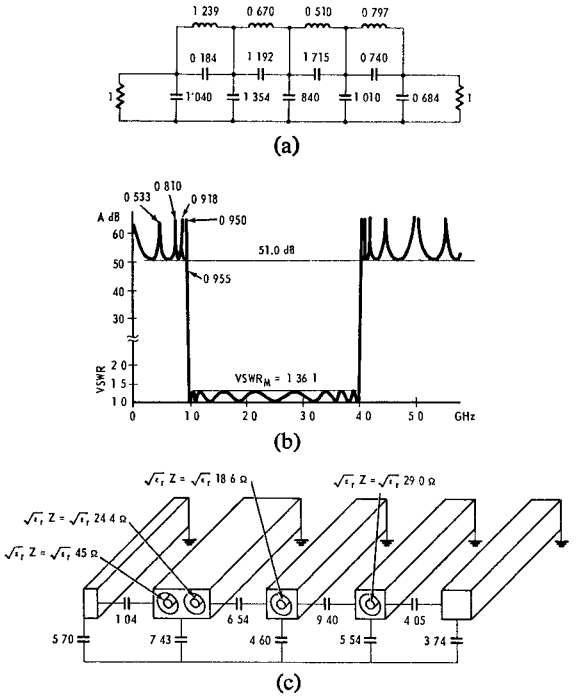

Fig. 8. Wide bandpass digital elliptic design. (a) Low-pass prototype. (b) Theoretical response characteristic. (c) Static capacitance values and series stub impedances.

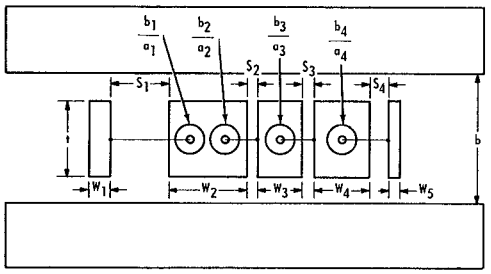

DIMENSIONS (INCHES)		
b = .500, t = .300		
S_1 = .237	W_1 = 085	b_1/a_1 = 2.95
S_2 = 050	W_2 = .269	b_2/a_2 = 1 80
S_3 = .033	W_3 = .172	b_3/a_3 = 1 56
S_4 = .078	W_4 = .228	b_4/a_4 = 2.00
	W_5 = 039	WITH $\sqrt{\varepsilon_r}$ = 1 44 (TEFLON)

Fig. 9. Sample cross-sectional dimensions for wide bandpass design.

tivity factor and the distributed filter selectivity factor is very slight.

For a 50-ohm realization, the self and mutual static capacitance values are obtained by substitution of the low-pass prototype element values in (T-6) and the series stub impedance values are obtained likewise from (T-8). The appropriate static capacitance network and stub impedance values are shown in Fig. 8(c). Dimensions for the coupled-line portion of the filter are obtained by use of (10) through (13) of Example I, and the stub impedances are obtained from the referenced nomograph [17]. A line drawing showing computed cross-sectional dimensions for $b=0.500$ inch and $t=0.300$ inch is shown in Fig. 9. The final realization takes the form shown in Fig. 2(b).

Conclusions

The digital elliptic distributed TEM filter is an extremely compact microwave structure capable of very sharp cutoff response in wideband applications throughout the frequency range up to X-band. The filter is finger-like in appearance, and realizes equal-ripple response in both passband and stopband as do elliptic-function lumped element filters; thus the name digital elliptic. The practical advantages and limitations of the digital elliptic filter are listed below.

Advantages

1) Existing tables [8]–[11] may be used to obtain prototype inductance and capacitance element values, thus circumventing tedious approximation and synthesis procedures.
2) The digital elliptic filter can be realized in a physical form identical to its lumped element prototype; thus no redundant elements nor equivalent circuit transformations are necessary.
3) Bandwidth scaling is accomplished by applying a multiplying factor to the tabulated element values; this simple recipe cannot be used in the exact design of most wideband microwave filters which employ quarter-wavelength elements.
4) The physical form is extremely compact, e.g., it is often four or five times smaller than an interdigital bandpass filter of comparable selectivity. It is also much more compact than other microwave realizations for elliptic-function response [7], [20].
5) The same design procedure holds equally well for either bandstop or bandpass designs, and the filter structural form is identical.
6) The digital elliptic filter has been found to give measured performance close to theoretical with relatively few adjustments.

Limitations

1) The structure is inherently wideband (>30 percent) and is not suited to narrowband designs due to physical limitations.
2) The structure requires series internal stubs and therefore more machined parts than some filter forms.
3) At X-band frequencies and above, practical ground plane spacings will result in junction effects which are difficult to compensate.

The practical design procedure for digital elliptic filters is extremely simple. All necessary equations are listed for handy reference in Table I. Two design examples, a bandstop and a bandpass, are given to demonstrate each step in the design.

References

[1] H. Ozaki and J. Ishii, "Synthesis of a class of strip-line filters," *IRE Trans. on Circuit Theory*, vol. CT-5, pp. 104–109, June 1958.

[2] A. I. Grayzel, "A synthesis procedure for transmission line networks," *IRE Trans. on Circuit Theory*, vol. CT-5, pp. 172–181, September 1958.

[3] R. J. Wenzel, "Exact design of TEM microwave networks using quarter-wave lines," *IEEE Trans. on Microwave Theory and Techniques*, vol. MTT-12, pp. 94–111, January 1964.

[4] B. M. Schiffman and G. L. Matthaei, "Exact design of band-stop microwave filters," *IEEE Trans. on Microwave Theory and Techniques*, vol. MTT-12, pp. 6–15, January 1964.

[5] M. C. Horton and R. J. Wenzel, "General theory and design of optimum quarter-wave TEM filters," *IEEE Trans. on Microwave Theory and Techniques*, vol. MTT-13, pp. 316–327, May 1965.

[6] P. I. Richards, "Resistor transmission-line circuits," *Proc. IRE*, vol. 36, pp. 217–220, February 1948.

[7] M. C. Horton and R. J. Wenzel, "Realization of microwave filters with equal ripple response in both pass and stop bands," presented at the Internat'l Symp. on Generalized Networks, Polytechnic Institute of Brooklyn, Brooklyn, N. Y., April 12–14, 1966.

[8] R. Saal and E. Ulbrich, "On the design of filters by synthesis," *IRE Trans. on Circuit Theory*, vol. CT-5, pp. 284–327, December 1958.

[9] R. Saal, "Der Entwurf von Filtern mit Hilfe des Kataloges normierter Tiefpässe," (The design of filters using the catalogue of normalized low-pass filters), Telefunken, G.M.B.H., Backnang/Württemberg, Western Germany, 1961.

[10] D. C. Pawsey, "Element coefficients for symmetrical two-section filters having Tchebycheff response in both pass and stop bands," *IRE Trans. on Circuit Theory*, vol. CT-7, pp. 19–31, March 1960.

[11] J. K. Skwirzynski, *Design Theory and Data for Electric Filters*. London: Van Nostrand, 1965.

[12] E. Ott, "A network approach to the design of multi-line 2N-port directional couplers," Polytechnic Institute of Brooklyn, Brooklyn, N. Y., Rept. PIBMRI-1236-64; Contract AF 30(602)-2868, Tech. Rept. RADC-TR-65-41, April 1965.

[13] R. J. Wenzel, "Exact theory of interdigital band-pass filters and related coupled structures," *IEEE Trans. on Microwave Theory and Techniques*, vol. MTT-13, pp. 559–575, September 1965.

[14] ——, "Theoretical and practical applications of capacitance matrix transformations to TEM network design," *IEEE Trans. on Microwave Theory and Techniques*, vol. MTT-14, pp. 635–647, December 1966.

[15] W. J. Getsinger, "Coupled rectangular bars between parallel plates," *IRE Trans. on Microwave Theory and Techniques*, vol. MTT-10, pp. 65–72, January 1962.

[16] E. G. Cristal, "Coupled circular cylindrical rods between parallel ground planes," *IEEE Trans. on Microwave Theory and Techniques*, vol. MTT-12, pp. 428–439, July 1964.

[17] *The Microwave Engineers' Handbook and Buyers' Guide*. Brookline, Mass.: Horizon House-Microwave, Inc., 1966, p. 91.

[18] G. L. Matthaei, "Interdigital band-pass filters," *IEEE Trans. on Microwave Theory and Techniques*, vol. MTT-10, pp. 479–491, November 1962.

[19] E. A. Guillemin, *Synthesis of Passive Networks*. New York: Wiley, 1957, p. 602.

[20] R. Levy, "Synthesis of distributed elliptic-function filters from lumped-constant prototypes," *IEEE Trans. on Microwave Theory and Techniques*, vol. MTT-14, pp. 506–517, November 1966.

On the Mode Correspondence Between Circular and Square Multimode Tapered Waveguides

CHARLES C. H. TANG

Abstract—**In an axially straight multimode circular waveguide taper excited with a pure TE_{11}° dominant mode, the first and only converted mode at and near cutoff is the TM_{11}° mode. It is shown that in an axially straight multimode square waveguide taper excited with a pure $TE_{10}^{\square}$ dominant mode, the $TM_{12}^{\square}$ mode corresponding to the TM_{11}° mode in circular case is not the only first converted mode at and near cutoff.**

The overall behavior or coupling mechanism of waveguides is similar whether the waveguide is rectangular, square, circular, or elliptical: i.e., the overall coupling coefficient at cutoff of a converted mode or modes approaches an infinity of the order $0^{-1/4}$.

Manuscript received October 24, 1966; revised December 19, 1966.

The author is with Bellcomm, Inc., Washington, D. C., formerly with Bell Telephone Laboratories, Inc., Holmdel, N. J.

[1] C. C. H. Tang, "Mode conversion in tapered waveguides at and near cutoff," *IEEE Trans. on Microwave Theory and Techniques*, vol. MTT-14, pp. 233–239, May 1966.

IN A PREVIOUS PAPER[1] it was shown that for the case of two-mode weak coupling the coefficient of coupling between the TE_{11}° dominant mode and the TM_{11}° mode in tapered circular waveguides tends to approach an infinity of the order $0^{-1/4}$ at cutoff frequency whereas the corresponding coefficient of coupling between the $TE_{10}^{\square}$ dominant mode and the $TM_{12}^{\square}$ mode in tapered square waveguides approaches instead a zero of the order $0^{1/4}$ at cutoff frequency. No convincing physical interpretation was given for such surprisingly drastically different coupling behaviors at cutoff frequency. It is the attempt of this paper to offer a convincing explanation.

For modes adjacent to the dominant mode, the mode correspondence between circular and square waveguides can be easily identified. As the mode order goes higher the identi-